PROCEEDINGS OF SPIE

An improved version of the Shadow Position Sensor readout electronics on board the ESA PROBA-3 Mission

V. Noce
M. Focardi
S. Buckley
A. Bemporad
S. Fineschi
M. Pancrazzi
F. Landini
C. Baccani
G. Capobianco
D. Loreggia
M. Casti
M. Romoli
L. Accatino
C. Thizy
F. Denis
Philippe Ledent

SPIE.

An improved version of the Shadow Position Sensor readout electronics on-board the ESA PROBA-3 Mission

V. Noce*[a], M. Focardi[a], S. Buckley[b], A. Bemporad[c], S. Fineschi[c], M. Pancrazzi[a],
F. Landini[a], C. Baccani[d], G. Capobianco[c], D. Loreggia[c], M. Casti[e], M. Romoli[d],
L. Accatino[f], C. Thizy[g], F. Denis[g], P. Ledent[g]

[a]INAF-OAA Arcetri Astrophysical Observatory, Largo E. Fermi 5, 50125 Firenze - Italy;
[b]Sensl, 6800 Airport Business Park, Cork - Ireland;
[c]INAF-OATo Turin Astrophysical Observatory, Via Osservatorio 20, 10025 Pino Torinese - Italy;
[d]University of Florence - Dept. of Physics and Astronomy, Largo E. Fermi 2, 50125 Firenze - Italy;
[e]ALTEC - Advanced Logistics Technology Engineering Ctr., C. Marche 79, 10146 Torino - Italy;
[f]AC Consulting, Via Trieste 16/b, 10098 Rivoli, Torino - Italy;
[g]CSL - Centre Spatial de Liège, Liège Science Park, 4031 Angleur, Liège - Belgium.

ABSTRACT

PROBA-3 [1] [2] is a Mission of the European Space Agency (ESA) composed by two satellites flying in formation and aimed at achieving unprecedented performance in terms of relative positioning. The mission purpose is, in first place, technological: the repeated formation break and acquisition during each orbit (every about twenty hours) will be useful to demonstrate the efficacy of the closed-loop control system in keeping the formation-flying (FF) and attitude (i.e. the alignment with respect to the Sun) of the system. From the scientific side, instead, the two spacecraft will create a giant instrument about 150 m long: an externally occulted coronagraph named ASPIICS *(Association of Spacecraft for Polarimetric and Imaging Investigation of the Corona of the Sun)* dedicated to the study of the inner part of the visible solar corona.

The two satellites composing the mission are: the Coronagraph Spacecraft (CSC), hosting the Coronagraph Instrument (CI), and the disk-shaped (1.4 m diameter) Occulter Spacecraft (OSC). The PROBA-3 GNC (Guidance, Navigation and Control) system will employ several metrological subsystems to keep and retain the desired relative position and the absolute attitude (i.e. with respect to the Sun) of the aligned spacecraft, when in observational mode.

The SPS subsystem [5] is one of these metrological instruments. It is composed of eight silicon photomultipliers (SiPMs), sensors operated in photovoltaic mode [6] that will sense the penumbra light around the Instrument's pupil so to detect any FF displacement from the nominal position.

In proximity of the CDR (Critical Design Review) phase, we describe in the present paper the changes occurred to design in the last year in consequence of the tests performed on the SPS Breadboard (Evaluation Board, EB) and the SPS Development Model (DM) and that will finally lead to the realization of the flight version of the SPS system.

Keywords: Metrology, Solar Physics, Coronagraph, Formation Flying satellites, SiPM – Silicon Photomultipliers, Readout electronics.

*noce@arcetri.astro.it; phone +39 055 275 5206

1. INTRODUCTION

The scientific payload of the PROBA-3 Mission is ASPIICS, a classical Lyot coronagraph where one of the two spacecraft (OSC) acts as an external occulter (EO). This giant, virtual instrument will take images of the inner solar corona in visible polarized light, from 1.08 $R_\odot$ up to about 3 $R_\odot$. The scientific objectives are mainly: 1) investigate the mechanisms driving the quiescent solar corona behavior and study the physical processes leading to coronal mass ejections (CMEs) and, 2) use the observations in order to predict the so-called "space weather" that can influence both ground and space-based electronic equipment. The external occulter that creates the artificial eclipse of the Sun is [8] a circular disk of 1.4 m diameter with a toroidal edge that will be used to block the light coming from the Sun disk but that will let pass the most of the coronal light. The telescope located on the CSC will thus be able to observe the solar corona closer to the limb than any other existing coronagraph.

PROBA-3 will follow a highly elliptic orbit around the Earth, with a perigee of about 600 km and an apogee of more than 68000 km. The duration of the orbit is about 20 hours, and the observations will take place around apogee, where the system is moving slower, in a timeframe of about 6 hours. During the observational period, the two spacecraft will form a single, giant (about 150 m), coronagraph producing a nearly ideal eclipse and allowing observations of the Sun corona.

During the remaining orbit time, the two spacecraft will lose the formation and will accommodate in a safe relative orbit, so to avoid any risk of collision. Before the beginning of the next observational phase, the two spacecraft will regain the formation using a series of metrological instruments that will let PROBA-3 to reach the desired relative positioning and system's attitude with unprecedented precision.

The PROBA-3 GNC will rely on several metrological systems to reach and maintain the correct relative position and attitude alignment: Star Trackers, RGPS (Relative GPS), VBS (Vision-Based Sensor), FLLS (Fine Lateral and Longitudinal System, Laser-based).

The CSC hosts two additional metrological subsystems:

- OPSE (Optical Position Emitters Sensors) that will exploit the image of a set of LEDs (Light Emitting Diodes) placed on the EO and imaged in the coronagraph instrument
- SPS, that is required to return a 3D position of the CSC with respect to the center of the umbra with an accuracy of 50 μm in lateral and 1 mm in longitudinal.
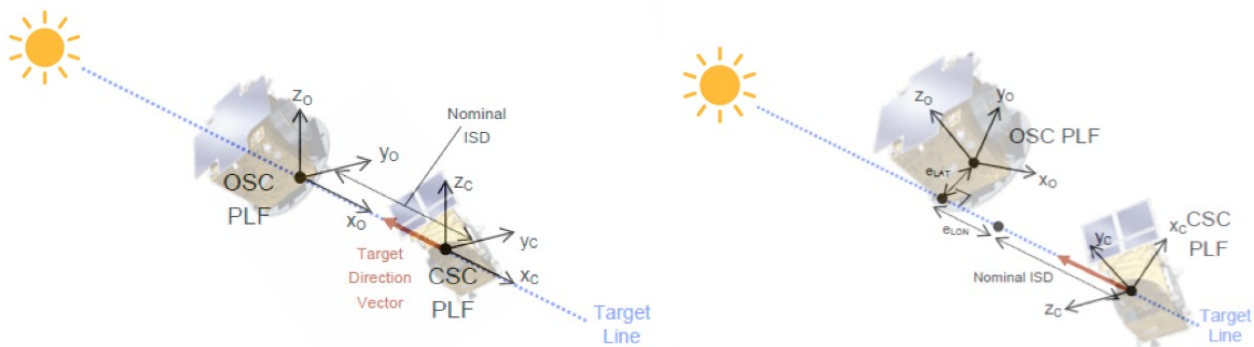

Figure 1: the PROBA-3 formation-flying satellites in nominal formation conditions (left) and in a generic situation with lateral and longitudinal position errors shown (right).

The Shadow Position Sensors system is composed by two sets of four SiPM (refer to Figure 2 for the two parts of the mechanical flange hosting the SiPM readout electronics) placed in a cross-like configuration at a distance of 55 mm from the coronagraph instrument's pupil center. The sensors will verify the correct centering of the entrance pupil in the shadow cone formed by the EO and shall measure the absolute position origin of the instrument with respect to the ideal position of the umbra center. A mechanical flange that is placed at the end of the optical tube contains the circular PCB that hosts the sensors and the electronics concerning the amplification, digitalization and transmission stages. The same flange supports the front door lid that is kept in closed position during the non-observational periods so to protect the instrument from the intrusion of the full Sun light. In case the door is closed, a set of SPS sensors will still be able to perform measurements thanks to their covering with neutral density filters.
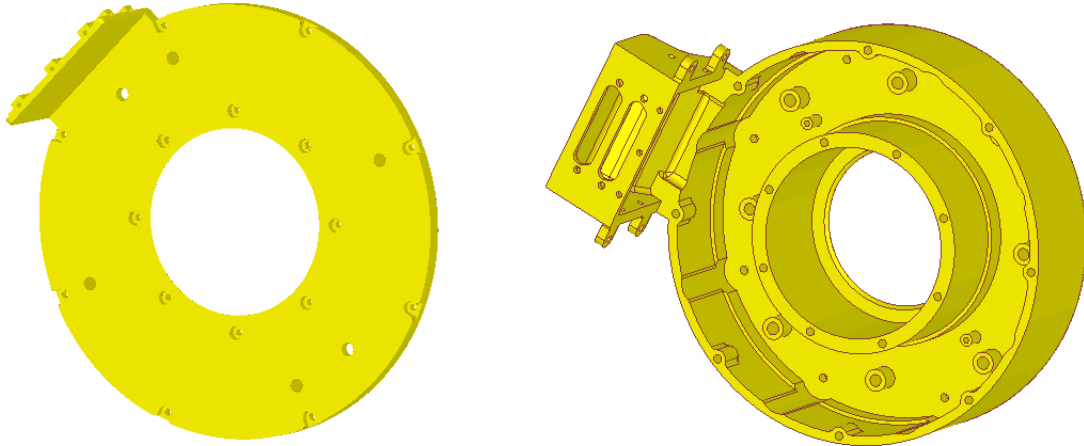
Figure 2: the SPS mechanical flange where are located the silicon photomultipliers and their readout electronics. The central hole, with the front vane, represents the ASPIICS Instrument input pupil.

2. SPS REQUIREMENTS SPECIFICATION

The following two requirements from ESA are the ones specifying the needed performance of the SPS in terms of lateral and longitudinal accuracy inside 3-D space regions. These requests will then need to be further translated in terms of dynamic range and resolution of measurements and, finally, in terms of current ranges and sensitivities.

A. "SPS performance requirement"

The Shadow Position Sensors (SPS) shall be used to verify that the Coronagraph Instrument's entrance pupil is centered within the umbra cone of the Occulter Disk. At the ISD (Inter-Satellite Distance) and within ±10 mm of the ideal position in lateral and ±100 mm in range, the SPS shall have a lateral measurement accuracy of 50 μm (3σ) in each axis, and a longitudinal measurement accuracy of 1 mm (3σ). These accuracies are with respect to the axis connecting the center of the Occulter with the center of the Sun.

B. "SPS performance goal"

The SPS should be able to return a 3D relative position measurement at reduced performance within a range of ±50 mm in lateral and ±500 mm in longitudinal (i.e. the SPS should always return a 3D measurement within a box of 100 mm in width and height and 1000 mm in depth, centered on the ideal position).

These two requirements, A and B, lead directly to the definition of two 3-D regions of space centered on each sensor's nominal position:
- *requirement box* (20 mm × 20 mm × 200 mm)
- *goal box* (100 mm × 100 mm × 1000 mm)

Starting from the knowledge of the power L (mW) present on the sensors at various points around the nominal position, these performances can be translated in requirements on both the dynamic range (referred to the *goal box*) and sensitivity (referred to the *requirement box*). Being that, thanks to an opportune narrowing of the light bandwidth, the power L is directly proportional to the current C (μA) generated by the SiPM, these conditions can be further translated in electrical quantities such as the current saturating the electronics and the achievable resolution.

2.1 Expected penumbra profile

A detailed study of the impinging power from the Sun and the corresponding generated current profiles, when in penumbra, has been performed in [7].

The calculation starts from a geometrical approximation of the light collected by a sensor at a given position, deriving from the intersection of a circle, representing the Sun disk, and an ellipse, accounting for the umbra projected by the External Occulter. This simplified model is then corrected with respect to the *limb darkening* effect. This effect consists in a wavelength-dependent variation of the spectral content of the light moving from the Sun center to its edge (limb). It can be shown that, in the visible range, the light coming from the Sun center is 1.3 times more intense than the average (computed on the overall disk) and the one coming from the limb is three times less. Being that the zones of interest in our study are the ones in which this physical phenomenon is more present, this effect has been fully taken into account in the calculation by means of a limb darkening function of the angle ϑ between the considered point on the disk and the line of sight:

$$\frac{I_\lambda(\vartheta)}{I_{\lambda 0}} = 1 - u_\lambda - v_\lambda + u_\lambda \cos\vartheta + v_\lambda \cos^2\vartheta$$

Where u_λ and v_λ are wavelength-dependent coefficients. In order to reduce the wavelength dependence and simplify the absolute radiometric calibration that will be realized covering a set of sensors with a neutral density filter (1% transmissivity), exploiting the full Sun as a "standard candle", the bandwidth has been reduced to 500-660 nm applying, for the computation of the expected power on the SPS, the following equation:

$$L = \int_{A_{pinhole}} \int_{\Omega_{SPS}} \int_{500}^{660} I_{\lambda 0}(1 - u_\lambda - v_\lambda + u_\lambda \cos\vartheta + v_\lambda \cos^2\vartheta)\, d\lambda\, d\omega\, dydz$$

2.2 SPS responsivity and current generated

The current generated on each sensor can be obtained convolving the power L by the sensors' responsivity $\varepsilon_{SPS}(\lambda,T)$ *(A/W)* that depends not only from the wavelength but also from the temperature. The last dependence is such that, in the range of temperatures foreseen in operational mode (29.8 - 40.7 °C), the resulting variations can seriously affect the desired measurement accuracy.

$$C = \int_{A_{pinhole}} \int_{\Omega_{SPS}} \int_{500}^{660} I_\lambda(\vartheta) T_W(\lambda) T_F(\lambda) \varepsilon_{SPS}(\lambda, T_{SPS})\, d\lambda\, d\omega\, dydz$$

Where T_W and T_F are the rad-hard window and the band-pass filter transmittances and T_{SPS} is the sensor's temperature.
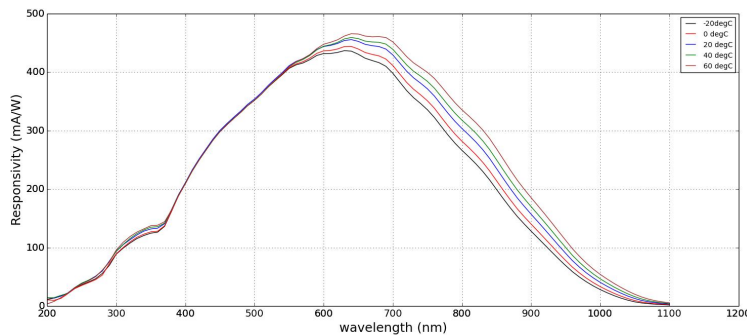

Figure 3: SPS responsivity curves as a function of wavelength and operational temperature (courtesy SensL).
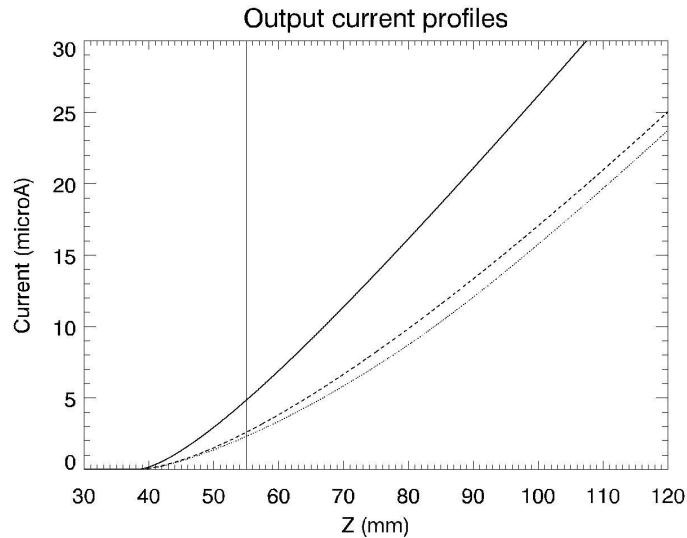
Output current profiles

Figure 4: output current profile integrated between 500 and 660 nm as a function of the distance from the umbra center and at the nominal ISD. The vertical line is located at the nominal position of SPS, namely 55 mm. The three plots correspond to: the geometrical case (solid), including the limb darkening (dashed) and considering a sunspot located at the limb (dotted).

The factor K *(W/A)* (SPS radiometric calibration function) that links the power L, as calculated in the previous paragraph, and the current C is $K = L / C$. Obviously, it is our interest to have this function K as much as possible constant. For this reason, the bandwidth of the optical filter has been optimized to tackle the two following potential problems:

1. In order to keep the responsivity as much as possible independent from temperature, so to avoid the introduction of such a parameter into the measurement (it is not possible a real-time access to the temperature measurements), the $\lambda > 660$ nm part of the spectrum has been eliminated. Moreover, this dependence could also affect the SPS calibration at full Sun, due to the likely increase in temperature of the whole system.

2. The limb darkening coefficients depend strongly from wavelength for $\lambda < 500$ nm, then the K conversion factor is far from being constant (the spectral content of light changes with heliocentric position). Again, this cut favors the reliability of the periodical in-flight calibrations.
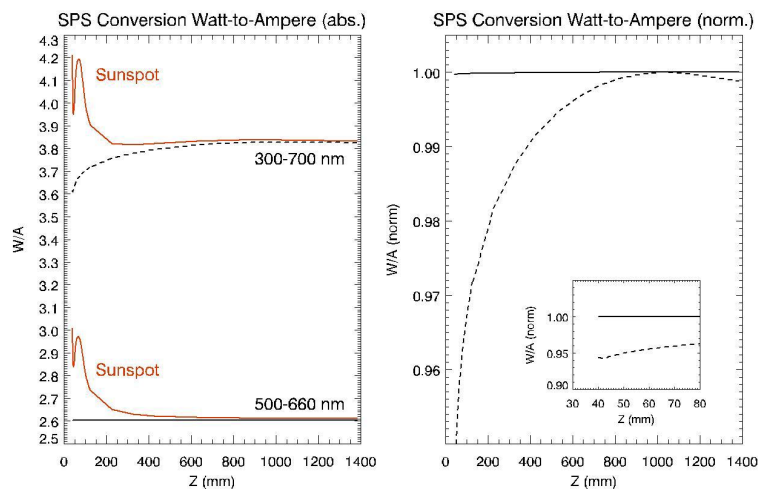

Figure 5: the figures show, for the two bandwidths 300-700 nm (dashed) and 500-660 nm (solid), the absolute (left) and relative (right) conversion factor K (W/A). The red curves refer to the case in which a sunspot is present on the limb.

From the figures above it is also apparent how one or more sunspots will influence the light spectral content, going closer to the penumbra limit. In these cases, the presence of sunspots counteracts the expected reduction of the *absolute* level of power.
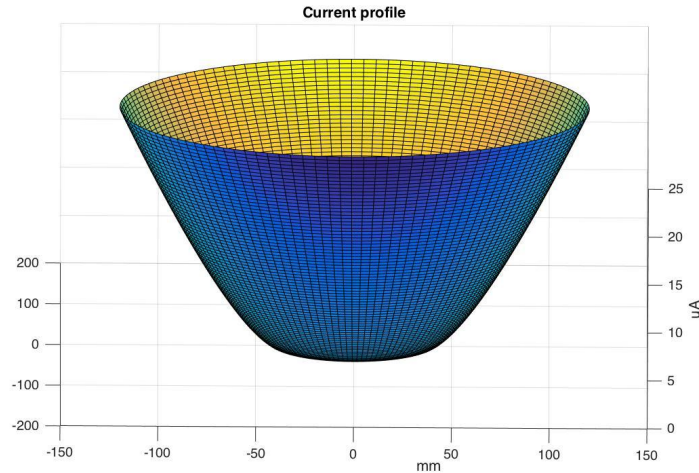

Figure 6: 3-D profile of currents in the 0-120 mm lateral range and at the nominal ISD.

2.3   Requirement flow-down

Starting from the knowledge of the power L, and being that the power is now directly proportional (factor K constant $\approx$ 2.60) to the current C generated by the SiPM, the ESA requirements A and B on both the dynamic range (referred to the *goal box*) and sensitivity (referred to the *requirement box*), see Fig. 8, can be further translated in electrical conditions such as the saturation of the electronics and the achieved resolution.

1. **"SPS dynamic range"**

   The Shadow Position Sensors (SPS) shall be able to provide a measurement of the levels of current up to 27 µA + margin.

This requirement states that the electronics shall not saturate for signals equivalent to the levels of power L present in the *goal box* (5.2% of full Sun) and descends from the ESA "B" requirement: *SPS performance goal*. The corresponding value of current present on the sensor when at the outer edge of the *goal box* is 27 µA. The same requirement assures also that in the smaller *requirement box* the electronics will provide significant measures.

2. **"SPS sensitivity for a lateral displacement of 50 µm"**

   The Shadow Position Sensor (SPS) electronics, up to a current of 6.3 µA, shall be able to provide the measurements with a sensitivity that, for the nominal position, is at least 0.5%.

This, and the following, requirement descends from the ESA "A" requirement: *SPS performance requirement*. It describes the needed sensitivity to detect a lateral displacement of 50 µm. This value of sensitivity is a representative one. Actually, the sensitivity varies in function of the absolute irradiance and its relative value is less demanding for lower values of power (3%) and 0.2% for the outer edge of the requirement box.
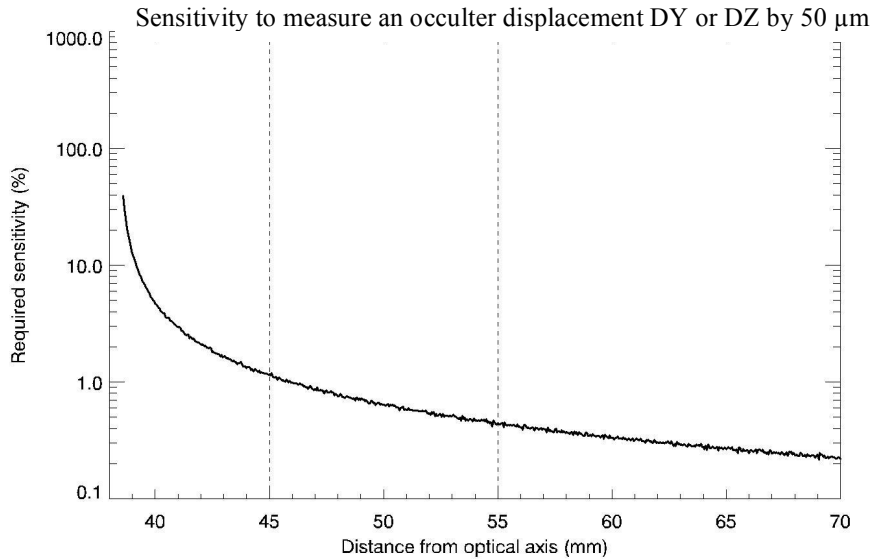
Figure 7: sensitivity required to detect the minimum lateral displacement of 50 μm as a function of the distance from the optical axis measured on the entrance pupil plane.

3. "SPS sensitivity for a longitudinal displacement of 1 mm"

The Shadow Position Sensor (SPS) electronics, up to 27 μA current shall be able to provide measurements with a sensitivity of at least 0.05%.

It must be noticed how the last requirement is about one order of magnitude more difficult to achieve than the previous one and, consequently, it can be stated that if the requirement #3 is satisfied, the requirement #2 is satisfied too.
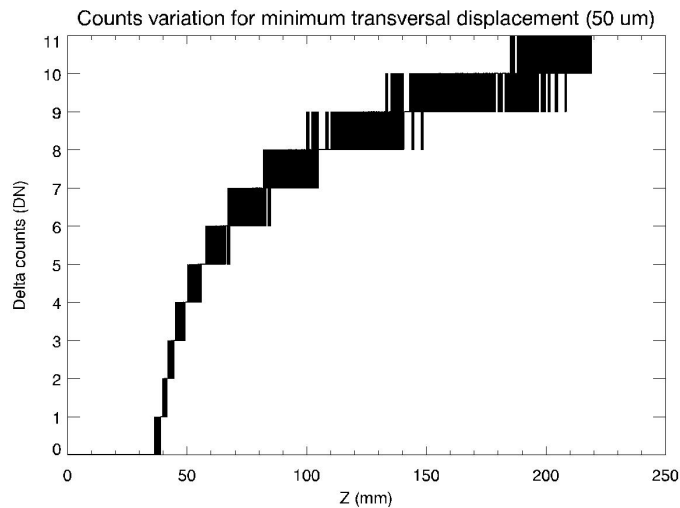

Figure 8: the sensitivity, in terms of LSB, for the minimum transversal displacement by 50 μm of a SPS sensor obtained with the adopted values of A_{TIA} and A_{HG}.

3. SPS DESIGN

The SPS readout electronics design evolved from the first models foreseen in the SPS model philosophy (Evaluation Board, EB and Development Model, DM) to the present one, at CDR stage. The new design was driven by laboratory tests on both the SPS Evaluation Board and Development Model and was oriented by analyses concerning the trade-off between complexity and benefits regarding, in particular, the opportunity to keep the stage subtracting a programmable voltage to the last stage [5].

3.1 SPS design

The design currently proposed by Sensl is a two-stages amplification chain as shown in Figure 9. The system relies on a double reading of a 12-bit serial ADC (Analog to Digital Converter) that digitizes the voltage of interest before and after a ×5 non-inverting amplifier in order to properly enhance the sensitivity at the lowest light levels and, at the same time, to satisfy the dynamic range requirement.
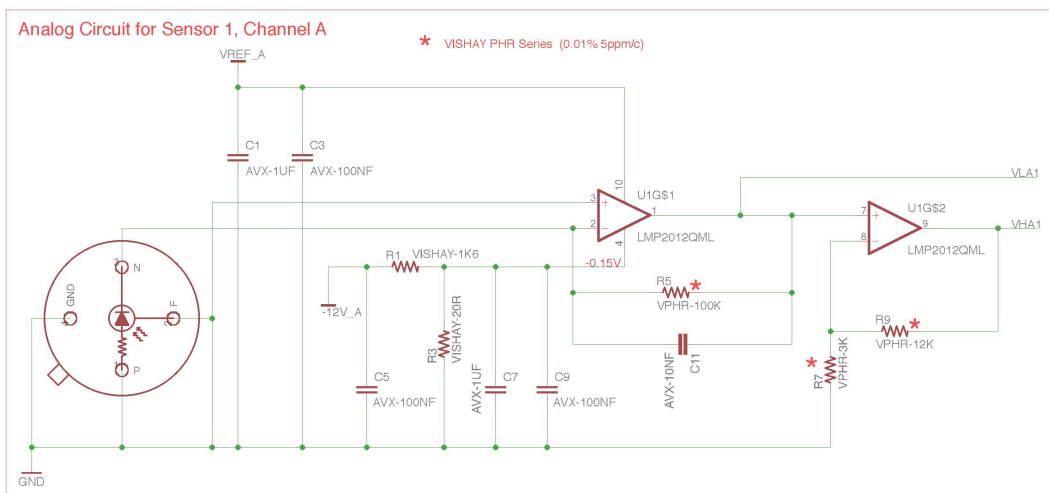

Figure 9: the amplification chain of one SiPM (CDR design).

3.2 Design parameters definition

Once established the maximum current level that we shall measure (27 µA) we can also theoretically compute the value of the feedback resistor of the transimpedance stage (first amplification stage): fixing R_f=100 kΩ (corresponding to a transimpedance gain A_{TIA}=100 kV/A) we have a margin on the currents of 85% and a margin in lateral range (mm) of 40%.

To properly select the second stage amplification factor A_{HG}, instead, we have to perform a trade-off between the corresponding amplification of the lower part of the current range and the part of the range that is amplified. In fact, if the input is between 0 and 50 µA, the second stage will enhance the lower $50/A_{HG}$ µA part of the range. Considering the value A_{HG}=5 will let, with respect to the maximum required of 6.7 µA, a 58% current margin and a 16% margin in lateral range.

Once fixed the two values A_{TIA} and A_{HG}, we can deduce important characteristics of the system such as e.g. the number of LSB corresponding to a sensor's displacement of 50 µm in a lateral direction in function of its distance from the penumbra center as in the following plot.

The physical quantity that is fed to the main SPS algorithms used to control the satellites' relative position is a digital number comprised between 0 and 20475 that is proportional to the *power*, measured in mW, given by the spectral irradiance (W/cm^2/nm) of the Sun, integrated on the pinhole surface (2.5 mm diameter) and on the transmissivity of the filters that will limit the wavelength band to the 500-660 nm interval. In the umbra cone (corresponding, for the nominal ISD of ≈144 m, to a distance from the Coronagraph pupil center less than 38.5 mm) the light flux is nearly zero (only

stray light is present [9]). When the sensors are outside the penumbra region they are exposed to full Sun. As reference, at the nominal SPS position (r_{SPS} = 55 mm and ISD) the light is about 0.47% of full Sun.

A functional scheme showing the conversion between physical quantities and the path followed by their measurements is shown in Figure 10 and explained in the following.
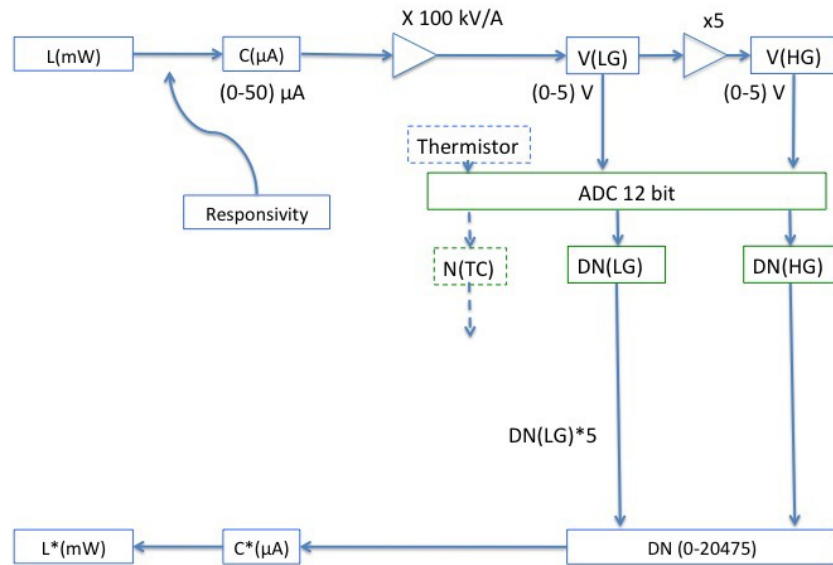

Figure 10: an illustration of the measurements and type of signals (currents and voltages) present along the stages of the SPS readout electronics.

Actually, the spectral content of the Sun light changes when moving from external positions to internal ones, where only a portion of the solar disk is seen, and the portion located on the Sun's edge becomes ever and ever more important. Shortly, we can state that the light becomes more and more "red". We have seen how this observation assumes a role in determining the optimal choice of the optical band-pass filter. Convoluting the responsivity of the sensor with the spectral solar irradiance (position dependent) we can obtain a current C measured in μA, considering the finite dimensions of the illuminated surface on the circular projection of the pinhole facing the sensor (2.5 mm diameter). This current C is the signal that needs to be translated in a voltage by means of a transimpedance amplifier.

In the electronic chain the transimpedance amplifier TIA converts the current C in a voltage V_{LG} compatible with the ADC input range 0-5V. The lower part of the voltage V_{LG} is amplified further by a non-inverting amplifier (gain A_{HG} =5) in a voltage V_{HG}.

Both the voltages V_{LG} and V_{HG} are digitized multiple times and their average is written in the 12-bit values DN_{LG} and DN_{HG} that are used to create single number DN simply adopting DN_{HG} for values lesser than 4000 (a value slightly less than 2^{12}) and multiplying DN_{LG} by 5 beyond this threshold.

The output of the readout chain is, then, a number DN comprised between 0 and 20475. This number is proportional to the current C and, due to the constancy of K, to the power L and so it can be fed to the algorithms used to compute the actual position.

The first stage amplification factor A_{TIA} was fixed with the aim of covering, with margin, the desired dynamic range, whilst the second stage amplification factor A_{HG} was chosen with the purpose of satisfying the sensitivity (or resolution) requirement. This factor cannot be raised indefinitely, considering that a too-high amplification factor would reduce the dynamic range of the amplified signals. In practice, the A_{HG} factor improves the resolution only in a region of signals equal to 5V/A_{HG}.

Finally, the SPS electronics design foresees, for each SiPM sensor, a thermistor to monitor the local temperature on the PCB; it is achieved thanks to a series resistor across the +5V supply providing an analog signal for the measured temperature. This signal is converted to digital by the 12-bit serial ADC and provided to the CSC as a housekeeping value.

3.3   Design changes from EB and DM

The EB adopted a single MICROFB-30035-X05 device. The DM hosted, instead, two complete sets of four MICROFC-30035 sensors on a circle of 55 mm radius and was very similar in shape and layout to the flight version [5].

Some changes on the electronics design were performed starting from the manufacturing of the Evaluation Board and Development Model and proceeding towards the final design [11], as hereunder itemized:

- In order to obtain an advantage from the point of view of the reduction of the Johnson noise, the amplification of the first two stages has been concentrated in the transimpedance stage only.
- The final stage has been simplified; removing the entire variable offset architecture, the Look-Up-Table and the DAC (Digital to Analog Converter). Previously, all the signal range benefited of an enhanced resolution, now this improvement concerns only the portion of signals where it is really needed.
- The OpAmp ADA4804-2 (previously OP484 in EB) has been changed in favor of LMP2012-QML, a device showing outstanding characteristics in particular regarding the bias current.
- The board hosts an entire section dedicated to the power switch, so that both sets can be powered independently and from two alternative voltage sources ±12V (main and redundant).
- Due to the availability of ±12V it is now possible to generate on-board a +5V voltage reference, being necessary to feed the ADC components to achieve the desired measurements accuracy.
- The SPS transmission lines have been changed to differential, so to increase the transmission reliability.
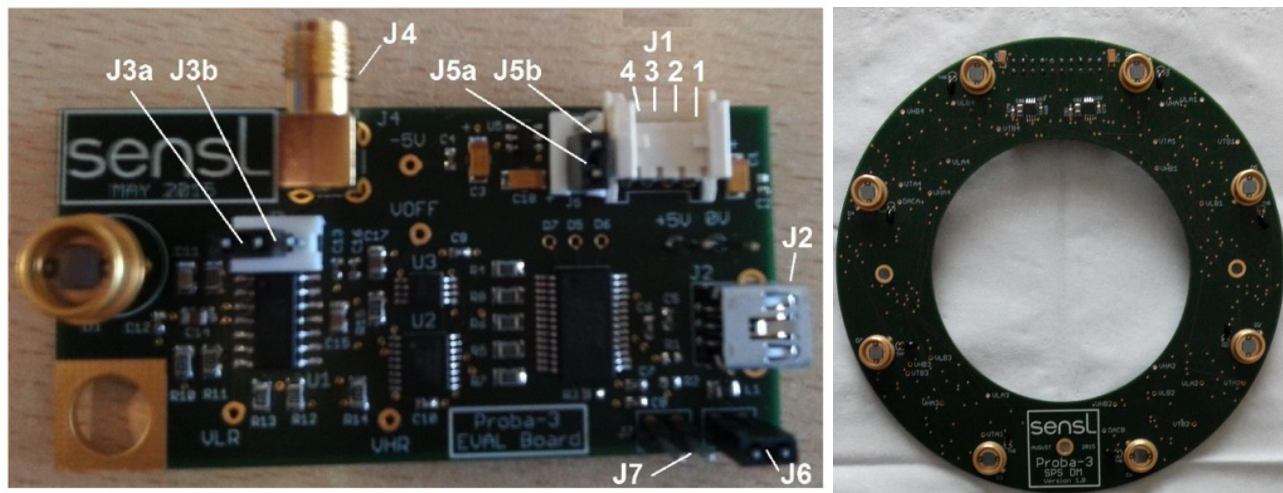

Figure 11: the SPS Evaluation Board (left) and the Development Model (right).

4.   CONCLUSIONS

In this paper we have illustrated the evolution of the SPS readout electronics design. The design changes have been properly put in relation with the SPS relevant requirements, leading us to an overall improvement of the electronics design and its expected performance.

5.   ACKNOWLEDGMENT

REFERENCES

[1] Renotte E. et al., "ASPIICS: an externally occulted coronagraph for PROBA-3. Design evolution", Proc. of SPIE Vol. 9143, 91432M, (2014).

[2] Renotte E. et al., "Design status of ASPIICS, an externally occulted coronagraph for PROBA3", Proc. of SPIE Vol. 9604, 96040A, (2015).

[3] Loreggia D. et al., "OPSE metrology system on board of the PROBA3 mission of ESA", Proc. of SPIE, Vol. 9604 96040F-1, (2015).

[4] Loreggia D. et al., "Characterization of the ASPIICS/OPSE metrology sub-system and PSF centroiding procedure", Proc. of SPIE AT+I, (2016).

[5] M. Focardi et al., "Formation Flying Metrology for the ESA-PROBA3 Mission: The Shadow Position Sensors (SPS) silicon photomultipliers (SiPMs) readout electronics", Proc. of SPIE, Vol. 9604 96040D-1, (2015).

[6] Jackson C., O'Neill K., Wall L., Mc Garvey B., "High-volume silicon photomultiplier production, performance, and reliability", SPIE Optical Engineering 53(8), 081909, (2014).

[7] Bemporad A., Focardi M., Capobianco G. et al., "The Shadow Positioning Sensors (SPS) for Formation Flying Metrology on-board the ESA-PROBA3 Mission", Proc. of SPIE, Vol. 9604 96040C-1, (2015).

[8] Landini F., Bemporad A., Focardi M. et al., "Significance of the occulter diffraction for the PROBA3/ASPIICS formation flight metrology", Proc. of SPIE, Vol. 9604, 96040E, (2015).

[9] C. Baccani et al., "Preliminary evaluation of the diffraction behind the PROBA-3/ASPIICS optimized occulter" Proc. of SPIE AT+I, (2016).

[10] G. Capobianco et al., "The satellite formation flying in lab: PROBA-3/ASPIICS metrology subsystems test-bed", Proc. of SPIE AT+I, (2016).

[11] V. Noce et al., "Metrology on-board PROBA-3: the Shadow Position Sensors (SPS) subsystem - Design and performance", IEEE Workshop on Aerospace Metrology, Padova (Italy), 21-23 June 2017 (2017).